Deplaine, H.; Acosta-Santamaría, VA.; Vidaurre, A.; Gómez Ribelles, JL.; Doblare Castellano, M.; Ochoa-Garrido, I.; Gallego Ferrer, G. (2014). Evolution of the Properties of a Poly(L-lactic acid) Scaffold with Double Porosity During In Vitro Degradation in a Phosphate-Buffered Saline Solution. Journal of Applied Polymer Science. 131:40956-40966. doi:10.1002/APP.40956.

Evolution of properties of a poly(L-lactic acid) scaffold with a double porosity during *in vitro* degradation in phosphate buffered saline solution

Harmony Deplaine[1†], Victor A. Acosta-Santamaría[2,3†], Ana Vidaurre[1,4*], José Luis Gómez Ribelles[1,4], Manuel Doblaré[2,4], Ignacio Ochoa[2,4], Gloria Gallego Ferrer[1,4]

[†] *These authors contributed equally to this manuscript*

[1]*Center for Biomaterials and Tissue Engineering, Universitat Politècnica de València, 46022 Valencia, Spain*

[2] *Group of Structural Mechanics and Materials Modeling (GEMM), Aragón Institute of Engineering Research (I3A), University of Zaragoza, 50009 Zaragoza, Spain*

[3] *Aragon Institute of Technology, 50009 Zaragoza, Spain*

[4] *Biomedical Research Networking Center in Bioengineering, Biomaterials and Nanomedicine (CIBER-BBN), 50018 Zaragoza, Spain*

[*]*Corresponding author. vidaurre@fis.upv.es Tel: +34 96 387 75 25 (Ext. 75253); Fax: +34 96 387 72 76.*

Abstract

A Poly(L-lactic acid) scaffold prepared by a combination of freeze extraction/porogen leaching methods was submitted to static degradation in phosphate buffered saline solution at pH=7.4 and 37 ºC for up to 12 months. After 6 months of degradation the scaffold maintained its integrity, although noticeable changes in permeability and pore size were recorded. After 12 months, SEM pictures showed that most of the trabeculae were broken and the sample disaggregates under minimum loading. Neither weight loss nor crystallinity changes in a first heating calorimetric scan were observed during the degradation experiment. However, after 12 months, a rise in crystallinity, from 13 % to 38 %, and a drop in Tg from 58 ºC to 54 ºC were measured in a second heating scan. The onset of thermal degradation moved from 300 ºC, to 210 ºC after 12 months. Although the elastic modulus suffered only a very slight reduction with degradation time, the aggregate modulus decreased 44 % after 6 months.

Keywords*: biomedical applications; degradation; mechanical properties*

INTRODUCTION

Tissue engineering, based on cell transplantation in combination with supportive porous scaffolds and biomolecules, is mainly focused on restoring the structure of tissue damaged by illness or traumatism. The porous scaffold serves as a three-dimensional template for initial cell attachment and subsequent tissue formation. The scaffold gradually degrades while the new tissue develops. It is

well known that scaffold architecture and mechanical properties have decisive effects on the regenerating tissue.[1] Changes in scaffold properties during degradation are of crucial importance in the long-term success of a tissue-engineered cell/polymer construct. The rate of degradation may affect many cellular processes, including cell growth, tissue regeneration and host response**.** Biodegradable scaffolds intended for tissue engineering must meet different requirements[2], including high porosity, adequate pore size and interconnected pore network, as well as having suitable mechanical properties. The scaffold should maintain the integrity of the designed structure and provide sufficient temporary mechanical support to withstand loading on the site of the implant.[3,4] The stress–strain response of the scaffold should be similar to that of the tissue surrounding the injured area, in order to deliver the appropriate mechanical signals to the cells to promote proper extracellular matrix production. Furthermore, as has been recently emphasized, the scaffold should remain at the site of injury until tissue formation, remodeling and maturation occur.[5]

Scaffold pore configuration, i.e. pore size, porosity and interconnectivity, is of special importance in the scaffold design.[6,7] Its permeability, closely related to pore interconnectivity, is also an important parameter, as it helps to control cell migration into the scaffold, as well as diffuse nutrients and waste products.[8,9]

Polylactide acid (PLA) undergoes hydrolytic degradation via random scission of the ester backbone. It degrades into lactic acid, a normal human metabolic by-product, which is broken down into water and carbon dioxide. Because hydrolytic degradation of aliphatic polyesters is autocatalyzed by carboxylic end groups generated by chain scissions of the ester bonds, solid films degrade faster than porous scaffolds and the degradation rate of the porous structures

increases with increasing pore wall thickness.[10-13] Porosity and pore size thus influence degradation and the release of degradation products.[14-16]

It has been established that PLA hydrolysis proceeds in three stage.[17,18] During the first stage aqueous solution penetrates the polymer, initiating hydrolytic degradation, mainly in the amorphous regions. At this stage a rapid decrease in molecular weight is observed but without significant mass loss, since the broken molecules are still not soluble in water and remain inside the sample. In the second stage, mass loss increases and lactic acid monomer formation is observed, with a slight change in molecular weight. At this time the long polymer chains are converted into shorter water-soluble fragments that dissolve into the medium (PLA becomes soluble in water for number average molecular weight (Mn) below 20.000 g/mol). Hydrolysis of soluble oligomers continues in the third stage until the polymer is totally hydrolyzed into monomer lactic acid. Polylactide acid is present in two stereopolymer forms: poly(L-lactide) acid (PLLA) and poly(D-lactide) acid (PDLA). Complete degradation of PDLA has been observed “in vivo” between periods of 10 months and 4 years, depending upon its molecular weight, degree of crystallinity, material shape and implantation site.[19] PLLA is more crystalline and has a lower degradation rate than PDLA.

PLLA has received approval from the US Food and Drug Administration (FDA) for human clinical use.[20] It exhibits mechanical properties suitable for human tissue engineering applications and has been widely used to guide the regeneration of bone and cartilage.[21-24] Its mechanical properties are affected by degradation from the start of the process. Vieira *et al*.[25] found that the decrease in tensile strength of PLA/PCL fibers follows the same trend as the

drop in molecular weight. Kang *et al*. [26] observed a linear fall in compressive strength from 10.5 MPa to 7 MPa in a 6-week degradation of porous PLLA scaffolds in SBF. Gaona *et al.* [27] studied hydrolytic degradation of PLA/PCL blend membranes showing the mutual influence of the degradation of both phases. Tsuji *et al*. [28,29] studied the hydrolytic degradation of PLLA films in PBS as a function of their crystallinity and found that the Young's modulus of the PLLA specimens decreased monotonously in the first 8 months. Interconnected porosity and pore size, followed by permeability, are the important factors in the mechanical properties of the scaffold.[30,31]. There is no agreement in the literature on the target mechanical properties of a scaffold for bone tissue engineering.[32] As stated by Rezwan *et al*.[33] in general the scaffold should have sufficient properties to avoid pores collapse when implanted. Human cancellous bone has a compressive strength of 4-12 MPa, a tensile strength of 1-5 MPa and an elastic modulus of 0.1-0.5 GPa[32]; and these properties can serve as guidance for the design of scaffolds. The initial mechanical requirements become less demanding with time of implantation because the regenerated tissue in the pores of the scaffold contributes to the mechanical properties and compensates the loss of scaffold's modulus caused by its degradation. There is also no established degradation rate; the recommendation is that the porous structure keeps its integrity during the first weeks after implantation.[32] *In vivo* experiments has demonstrated higher degradation rates than *in vitro*.[15]

In a previous work, our group proposed a porous PLLA scaffold with double porosity: micropores generated by dioxane solvent using a freeze extraction technique and macropores produced by the leaching of macroporogen spheres. A study was carried out on the influence of the preparation parameters on its

structure and mechanical properties[34] and the material has been proposed for cartilage[35] and bone regeneration after being coated with a biomimetic apatite layer[36]. In this work we studied the evolution of the properties of the PLLA scaffold after different degradation times in a phosphate buffered saline solution. The novelty of the present study is that the scaffold preparation method allows PLLA to crystallize to its maximum capacity. This high crystallinity is reached during the removal of the porogen with ethanol at 37ºC and has an important role in the evolution of the scaffold's properties with degradation time. Although we have seen changes in the molecular weight with the time of degradation no mass loss was recorded, as chains remain entrapped in the crystalline regions. The high crystallinity of our scaffold also hinders the incorporation of those degraded chains in the crystals, as usually occurs in lower crystalline scaffolds found in the literature. We here emphasize these novel aspects in the degradation of this highly crystalline PLLA scaffold.

MATERIALS AND METHODS

Materials

Medical grade poly(L-lactic acid) (PURASORB PL 18) (PLLA) with a viscosity of 1.8 dl/g and an average molecular weight M_w=165000 g/mol was purchased from Purac Biomaterials (The Netherlands). Poly(ethyl methacrylate) (PEMA) spheres from Elvacite (Elvacite 2043 acrylic resin) with diameters ranging from 120 to 200 μm were used as macroporogen and 1-4 dioxane (98 % pure) from Sigma Aldrich was used as PLLA solvent and microporogen. Ethanol (99 % pure) from Scharlab was used as a low temperature solvent of the dioxane.

Preparation of the PLLA scaffold

The PLLA scaffold was prepared by a combination of the freeze extraction/porogen leaching methods.[37,38] A solution of PLLA in 1-4 dioxane with a 15 wt.% of PLLA was homogeneously mixed at room temperature with the PEMA spheres in mass proportion 1:1 (w:w) in a Teflon mould and immediately frozen with liquid nitrogen. Cold ethanol at -20 ºC was then poured on the frozen sample to dissolve the crystallized dioxane. Dioxane extraction was conducted in a cold ethanol bath at -20 ºC in which the ethanol was renewed at least four times. Then extraction of the PEMA porogen was carried out with ethanol at 40 ºC under slow stirring. The ethanol was changed until no PEMA deposit was left on a glass when a drop of the extraction liquid was evaporated. After extraction, the scaffold was dried in an air atmosphere for 24 h and then in vacuum to constant weight, first at room temperature and later at 40 ºC. Cylinders 6 mm in diameter and 4 mm high were punched from larger pieces of scaffold.

Degradation experiments

Each sample of known mass was immersed in 2 ml of a phosphate buffered saline solution (PBS) at 37 ºC and maintained for 3, 4.5, 6 and 12 months under static conditions. The PBS bath was renewed every 2 weeks. After different immersion times in PBS, three replicates were washed several times with distilled water with gentle shaking, then dried (as described above) and weighed. The mass loss of the different scaffolds with time of degradation was evaluated as follows:

$$\mathrm{mass\,loss}\,(\%) = \frac{m_i - m_f}{m_i} \cdot 100 \qquad (1)$$

where m_i is the initial and m_f the final mass of the samples. A balance (Mettler Toledo) with a sensitivity of 0.01 mg was used to weigh the samples, which were then analysed by different methods to determine the influence of degradation time on the scaffold properties.

Scanning electron microscopy (SEM)

The morphology of the samples was analyzed with a JEOL JSM 6300 scanning electron microscope at an accelerating voltage of 15 kV. The samples were mounted onto copper holders and gold sputtered for observation. Scaffold sections were excised with a razor blade in order to observe both the surface and cross section.

Microtomography (µCT)

Microtomography was carried out to define average macropore size. The image files (DICOM- Digital Imaging and Communication in Medicine) provided by the µCT were the main input for building the geometric model of the scaffold. Images of the whole sample were obtained by 360º rotational scanning. A GE Healthcare eXplore locus SP µCT was used, with an X-ray filter number 2, 45 kV voltage and 120 mA power. The resolution of the equipment was 8 µm. 90 DICOM files were obtained for each sample (one image for each 4.0º rotation). Five replicates for each degradation time (0, 3, 4.5 and 6 months) were measured to determine the corresponding macropore size.[37]

Mechanical properties under compression

The mechanical properties of the degraded scaffolds were measured under wet conditions in two static uniaxial tests: unconfined (UC) and confined compression (CC).[34] During the UC test, the scaffold can generate a lateral deformation when a load or displacement is applied. In the CC test the lateral

deformation of the scaffold is constrained, due to the sample being in a confined space. Mollica *et al*.[40] describe the development of a typical stress–strain curve for scaffolds submitted to uniaxial compression tests. After the first small region in which the struts and plates are being compressed, once a critical load has been reached, they buckle giving way to a plateau region, in which the apparent density of the material grows until the stress–strain curve increases again (third region) until failure or total collapse of the structure.[40] For the UC and CC tests, either apparent Young's modulus (E_S) or the aggregate modulus (H_A) were calculated, respectively, from the slope of the first linear region of the stress–strain curve and with the initial cross-section area.[34] Additionally, the yield strength (Y) was determined between the first and second region. For this study, the first point after the linear region at the stress-strain curve was determined as the lower yield limit (Y_L), at which plastic deformation begins to occur.[41]

Before carrying out the wet compression tests, the samples were maintained in PBS solution for 24 hours at a temperature of 37 °C.[40] The tests began with a predeformation of 4 % of the total thickness of the sample at 0.001 mm s^{-1}, in order to eliminate the nonlinearity generated by the geometrical variability of the samples and to normalize an initial reference test point.[34,43] A monotonic ramp performed at a 0.01 mm s^{-1} cross-head velocity was carried out using an Instron MicroTester 5548 with a precision of 0.0001 N and 0.001 mm force and displacement, respectively, and provided with a 50 N load cell.[34] The dimensions of the sample were measured before and after the test. Five replicates for each degradation time and UC and CC test were measured to determine the corresponding E_S, H_A and Y_L modulus. Finally, Poisson's ratio (ν)

describes the lateral expansion during axial compression, defined as the ratio between lateral and axial strains. For each degradation period, ν can be deduced from the E_S and H_A averaged data, using the theory proposed in[44-46] and according to the equation:

$$E_S = \frac{(1+\nu)(1-2\nu)}{1-\nu} H_A \quad (2)$$

Permeability

Permeability is measured by quantifying the ability of a porous medium to conduct fluid flow through its interconnected pores when subjected to pressure[47,48], regardless of the fluid used in the measurement and the thickness of the porous sample.[49,50]

The permeability test was developed under conditions for which Darcy's Law (Eq. 3a) is valid, i.e. for Reynolds numbers lower than 8.6: [34,47-51]

$$k = \frac{\mu \cdot t}{A} \frac{Q}{\Delta p} \quad (3a)$$

$$\Delta p = \Delta p_{scaffold} - \Delta p_{chamber} \quad (3b)$$

where k is the intrinsic permeability (m^2), μ the dynamic fluid viscosity (deionized water $\mu=10^{-3}$ Pa s), t the specimen thickness, A the cross-sectional area, Q the volumetric flow rate and Δp the total pressure drop across the scaffold sample (Pa). The total pressure drop measured with the scaffold specimen inside the chamber is $\Delta p_{scaffold}$, whereas $\Delta p_{chamber}$ is the measurement for the empty chamber (Eq. 3b).[52] Due to the test configuration, the measured pressure drop is attributed to the scaffold microstructure and the section change. The $p_{scaffold}$ and $\Delta p_{chamber}$ were measured between two points of the permeameter chamber using a pressure meter (Testo 510 with a precision of ± 0.1% and operating range from 0 to 2000 hPa). Five samples comprising

cylinders of 6 mm diameter and 3.02 ± 0.02 mm thick were tested for each degradation period. In accordance with the experimental protocol, the fluid flow through the scaffold was varied by controlling the flow rate (20, 40, 60 ml min^{-1}).[34] The $\Delta p_{scaffold}$ generated in each case was measured and then averaged out to determine the permeability of the structure, using Eq. (3a).

Differential scanning calorimetry (DSC)

The thermal properties of the scaffolds were determined by a Pyris 1 calorimeter (Perkin Elmer). Dry nitrogen gas was passed through the DSC cell at a flow rate of 20 ml/min. The temperature of the equipment was calibrated with the melting points of indium and zinc. The heat of fusion of indium was used for calibrating heat flow. Each sample underwent two heating processes from 0 ºC to 21 0 ºC at a rate of 10 ºC/min. The samples were cooled between scans from 210 ºC to 0 ºC at a rate of -10 ºC/min. The data from all three scans were collected for subsequent analysis. The first scan measured the effect of the previous history of the material (in our case the scaffold preparation followed by the degradation processes). As all the samples had been melted and crystallized under the same conditions, the second heating scan depended on the material properties.[53] Crystallinity was assumed to be proportional to the experimental heat of fusion, according to:

$$\mathrm{x_c}(\%) = \frac{\Delta \mathrm{h_m}}{\Delta \mathrm{h_m^0}} \times 100 \qquad (4)$$

where Δh_m is the measured enthalpy of fusion of the sample, Δh_m^0 = 93.1 J/g is the enthalpy of fusion of the completely crystalline material (i.e. corresponding to an infinite thickness crystal).[54,55]

Gel permeation chromatography (GPC)

The weight average molar mass of the samples was determined with a gel permeation chromatographer at 30 ºC using a Waters Breeze GPC system with a 1525 Binary HPLC pump (Waters Corporation, Milford, MA) equipped with a 2414 refractive index detector and Waters Styragel HR THF columns. THF was used as the eluent at a flow rate of 0.5 ml/min. The calibration curve was prepared by using monodisperse polystyrene standards from Shodex (Showa Denko K.K., Kawasaki, Japan).

Thermogravimetric analysis (TGA)

TGA analysis (Thermogravimetric analyser SDTQ600 from TA Instruments) was performed to evaluate the effect of the static degradation in PBS on the thermal stability of the scaffolds. The samples were subjected to a temperature ramp from room temperature up to 800 ºC at 20 ºC/min under nitrogen flow (50 ml/min).

Statistical analysis

For the experimental data (E_S, H_A, Y_L and k), a normal distribution was tested by the Anderson-Darling test. One-Way ANOVA was performed for parametric comparison. Statistical significance was set at a mean of $p<0.05$ with 95% confidence intervals.[46] The statistical methods applied were calculated using Minitab software. Finally, the results were presented as mean ± standard deviation.

RESULTS

Morphology of the scaffolds

As can be seen in the SEM micrographs of the samples sections in Fig. 1, the macro and microstructures of the different scaffolds submitted to different periods of degradation do not present significant changes up to 6 months. The

trabeculae seem to be intact and the macropores appear to maintain their size and interconnectivity. However, a significant change was observed after 1 year, when most of the trabeculae were seen to be broken in the SEM pictures, in fact at this time they disaggregate easily when manipulated. No changes in the micropore dimensions were observed for any degradation time, even after 1 year of incubation in PBS. No morphological differences were observed between the section and surface of the scaffolds.

Table 1 shows average macropore size as determined by µCT. In contrast to what was observed in the SEM pictures, µCT shows that pore dimension increased with degradation time (82,81 % after 6 months). Moreover, the statistical treatment found significant differences ($p<0.05$) between the initial condition and all degradation times (t_1 = 3, t_2 = 4.5 and t_3 = 6 months, respectively). Significant differences were also found at t_3 with regard to the t_1 and t_2 degradation periods.

Table 1 –Evolution of macropore size, permeability, and apparent Young's modulus for the UC (E_S) and aggregate modulus for the CC (H_A) tests, as a function of degradation time for PLLA scaffold under static conditions.

Degradation time (months)	**Macropore size (μm)**	***Unconfined test - UC***			***Confined test - CC***			ν	**k (m^2)**
		E_S (MPa)	**Stress Y_L (MPa)**	**Strain Y_L**	**H_A (MPa)**	**Stress Y_L (MPa)**	**Strain Y_L**		
t_0 = 0	127 ± 5	3.43 ± 0.25	0.38 ± 0.08	0.17 ± 0.02	7.73± 0.67	0.34 ± 0.06	0.05 ± 0.01	0.41	$1.20\times10^{-10} \pm 7.71\times10^{-12}$
t_1 = 3	184 ± 10	3.06 ± 0.12	0.41 ± 0.07	0.16 ± 0.02	5.46± 0.95	0.24 ± 0.04	0.05 ± 0.01	0.37	$1.77\times10^{-10} \pm 2.96\times10^{-11}$
t_2 = 4.5	206 ± 2	2.94 ± 0.33	0.30 ± 0.09	0.15 ± 0.02	4.56 ± 0.84	0.35 ± 0.09	0.06 ± 0.01	0.34	$2.97\times10^{-10} \pm 3.74\times10^{-11}$
t_3 = 6	232 ± 8	2.5 ± 0.30	0.23 ± 0.03	0.15 ± 0.03	4.31 ± 0.96	0.34 ± 0.05	0.10 ± 0.02	0.36	$3.18\times10^{-10} \pm 5.79\times10^{-11}$

E_S = Young modulus

H_A = Aggregate modulus

Y_L = Lower yield limit point

v = Poisson's ratio.

k = Permeability

Degradation Time (months)	Macroporosity	Microporosity
$t_0 = 0$	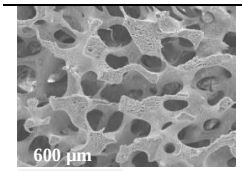	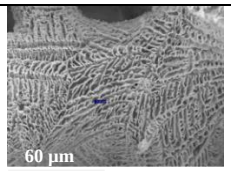
$t_1 = 3$	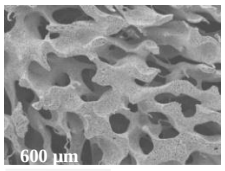	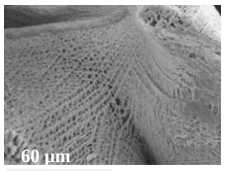
$t_2 = 4.5$	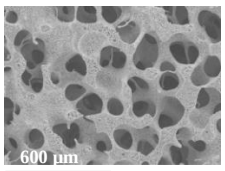	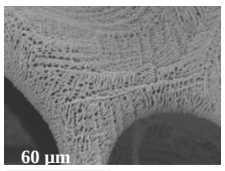
$t_3 = 6$	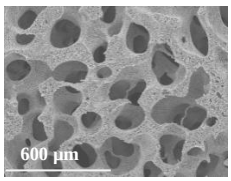	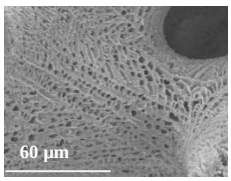
$t_4 = 12$	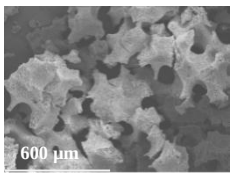	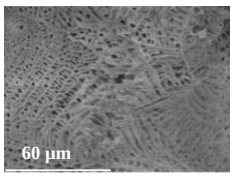

Fig. 1 – SEM pictures at different magnifications and degradation times of the section of the PLLA scaffold showing the effect of static degradation in PBS on scaffold morphology. The pictures on the surface of the scaffolds are similar to these ones.

Mass evolution

Mass loss as a function of degradation time was determined by applying Eq. (1). There were no significant changes in the sample mass for the first 6 months of degradation in PBS and only 2 % of mass loss was measured after 1 year.

Mechanical properties

The influence of the static degradation experiment on the mechanical properties of the PLLA scaffold was evaluated by a compression test (unconfined UC and confined CC), from which the elastic modulus was calculated (see the representative stress versus strain curves for each time of degradation in Fig. 2 and the calculated mean parameters in Table 1).

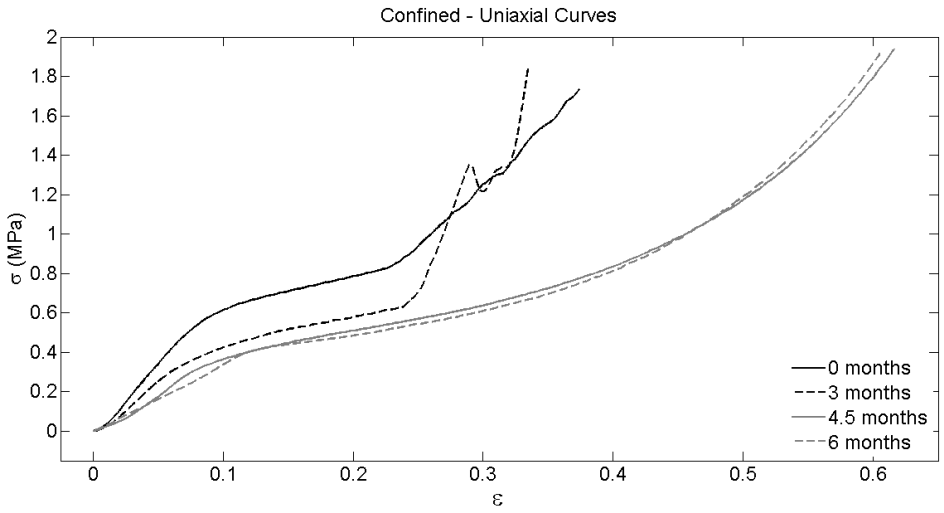

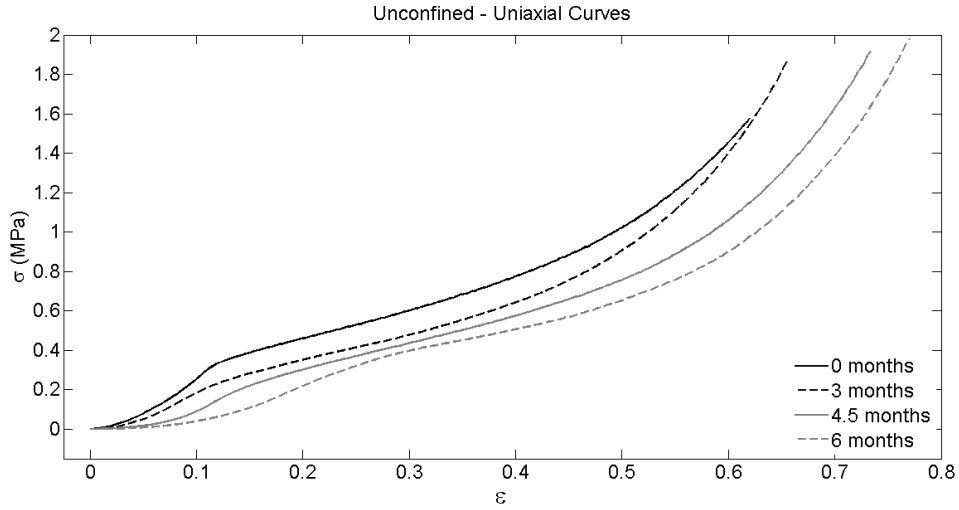

Fig. 2 – Stress–strain curves of the confined and unconfined uniaxial compression tests after 0, 3, 4.5 and 6 months of static degradation for the PLLA scaffolds.

The apparent Young modulus (E_S) and the aggregate modulus (H_A) decreased with degradation time. E_S was reduced by 27.16 % between the initial and final immersion period (from E_S (t_0)= 3.43 ± 0.25 MPa to E_S (t_3)= 2.50 ± 0.30 MPa). H_A was reduced by 44.27 % (from H_A (t_0)= 7.73 ± 0.67 MPa to H_A (t_3) = 4.31 ± 0.96 MPa). The ν factor was also seen to decrease with degradation time (Table 1).

For UC, the strain required to achieve the lower yield limit (Y_L), was higher than that reported in the CC test (Table 1) and it was seen to decrease with degradation time (11.08 % between t_0 and t_3). This trend was opposite to the strain data reported in the CC tests, in which deformation increased by 97.5 % (between t_0 and t_3). However, in both cases at t_3, and considering the experimental dispersion, the plastic zone started at the same strain level. Significant differences were found in the CC results between t_3 and the t_0 and t_1

degradation periods ($p<0.05$). In the UC test, the obtained stress level for Y_L decreased between t_0 to t_1, while the CC data showed the opposite trend. After the t_1 degradation period, the Y_L stress results showed a change of tendency in both the UC and CC tests (Table 1).

Permeability

The results of the permeability test are shown in Table 1. The intrinsic permeability (*k*) of the scaffold structure can be seen to increase with immersion time. After 6 months' degradation permeability rose by 165.23 % (k (t_0)= 1.20 x 10^{-10} to k (t_3)= 3.18 x 10^{-10} m^2) accompanied by increased experimental dispersion. The results at t_3 showed the highest dispersion with ± 5.79 x 10^{-11} m^2 (Table 1). The statistical treatment determined significant differences ($p<0.05$) for *k* values between the initial condition and the t_2 and t_3 degradation periods (4.5 and 6 months, respectively), with no significant differences between them (t_2 and t_3).

Calorimetric properties

The influence of the static degradation process on the calorimetric properties of PLLA scaffold was evaluated by DSC scans. Crystallinity after the first heating scan is representative of the thermal history of the sample (porous scaffold fabrication and degradation), while that taken from the second heating scan (2) is representative of the properties of the previously degraded and melted bulk sample. The degraded scaffolds present a double melting peak in the first scan (Fig. 3). The second heating scan shows differences with the first one; two crystallization peaks appear, cold crystallization takes place around 100 ºC, but a smaller exotherm appears at higher temperatures with a minimum of around

160 ºC. The second crystallization peak is characteristic of PLLA samples crystallized at low temperatures (as it is the case of the crystals formed during heating at temperatures immediately above the glass transition) and is explained by a recrystallization process.[56] The double melting peak does not appear in the second heating scan, while the maximum of the melting peak appears at a lower temperature in the second heating scan. This could be due to a decrease in molecular weight producing thinner, less perfect lamellae.[57]

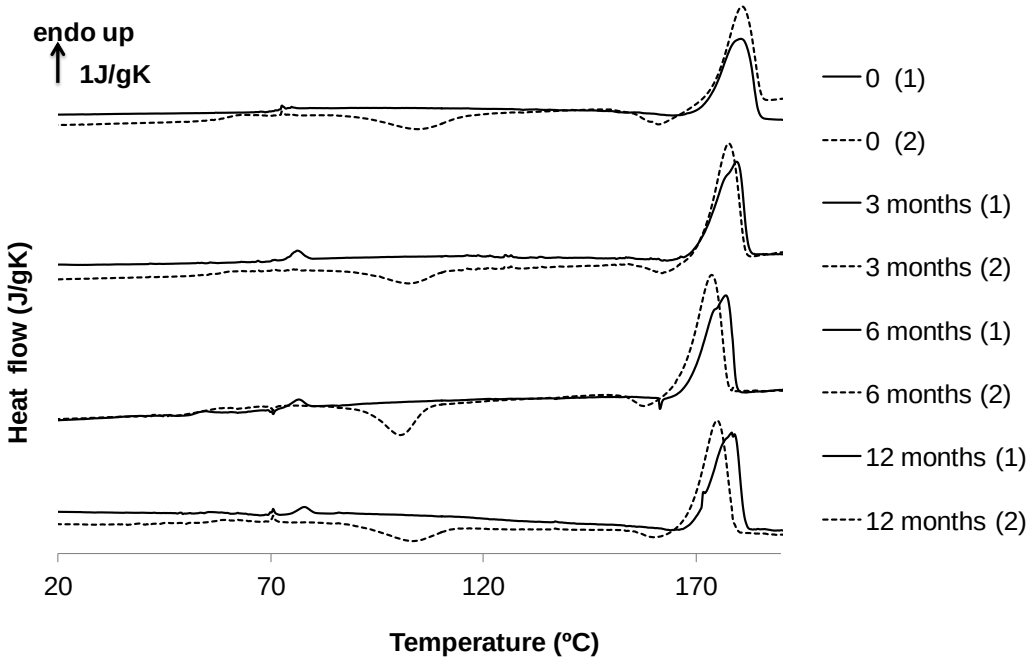

Fig. 3 – Normalized heat flow of the DSC first (1) and second (2) heating scans after 0, 3, 6 and 12 months of static degradation of PLLA scaffolds. The heat flow was normalized by the mass of the samples and the heating rate (10 ºC/min). The arrow represents a unit of heat flow in J/gK.

The enthalpic glass transition temperature (determined as the intersection temperature of the enthalpy lines at the liquid and glassy states in the enthalpy

vs. temperature diagram) was calculated from these curves (Table 2). The crystallinity values after the first and second heating scans are presented in Table 2 as well. They were calculated by integrating the heat flow trace with respect to a baseline joining a point immediately above the glass transition and one after the melting. This way the crystallinity values obtained after the second scan corresponds to the crystallinity obtained in the cooling scan, after the first melting. An endothermic peak appears in all the degraded samples overlapped on the glass transition process but not in the non-degraded ones. This peak is associated to the physical ageing suffered by the amorphous phase of the semicrystalline samples annealed for quite long times at 37 ºC which is around 30 degrees below its glass transition. This peak disappears in the second scan since the samples are heated immediately after cooling from high temperatures. It is worth note the small value of the heat capacity increment at the glass transition, Δc_p, in the first scan due to the high crystallinity of the sample. The scaffold glass transition temperature (T_{g2}) and crystallinity (x_{c2}) at the second heating are smaller than in the first one for all degradation times, and consequently Δc_p at T_g is higher in the second scan than in the first one. Glass transition temperature at day 0 shifted from 72 ºC in the first scan to 58 ºC in the second. Crystallinity and glass transition values in the first heating scan after the different degradation times remained almost constant. In the second scan, crystallinity increased with degradation time, from 13 % in the non-degraded sample up to 38 % after 1 year's degradation.

Table 2–Crystallinity (x_c (%)) and glass transition temperature (T_g) after the first (1) and second (2) DSC scan of scaffolds after different static degradation times in PBS at 37ºC.

Degradation time (months)	Crystallinity (%)		Glass transition Temperature (ºC)	
	x_{c1}	x_{c2}	T_{g1}	T_{g2}
t_0 = 0	48	13	72	58
t_1 = 3	46	22	72	58
t_3 = 6	51	27	73	54
t_4 = 12	49	38	75	54

Gel permeation chromatography

From the molecular weight distribution functions obtained by GPC (Fig 4) it is possible to analyze the effect of degradation time on the weight average molar mass (Mw) and the PLLA polydispersity index (Mw/Mn) (results shown in Table 3). The non-degraded PLLA scaffold presents a narrow molecular weight distribution function, with its maximum around 2 10^5 g/mol. A higher fraction of short chains is generated with degradation time and the weight average molar mass decreases. The polydispersity index rises as the GPC curves broaden to lower molecular masses.

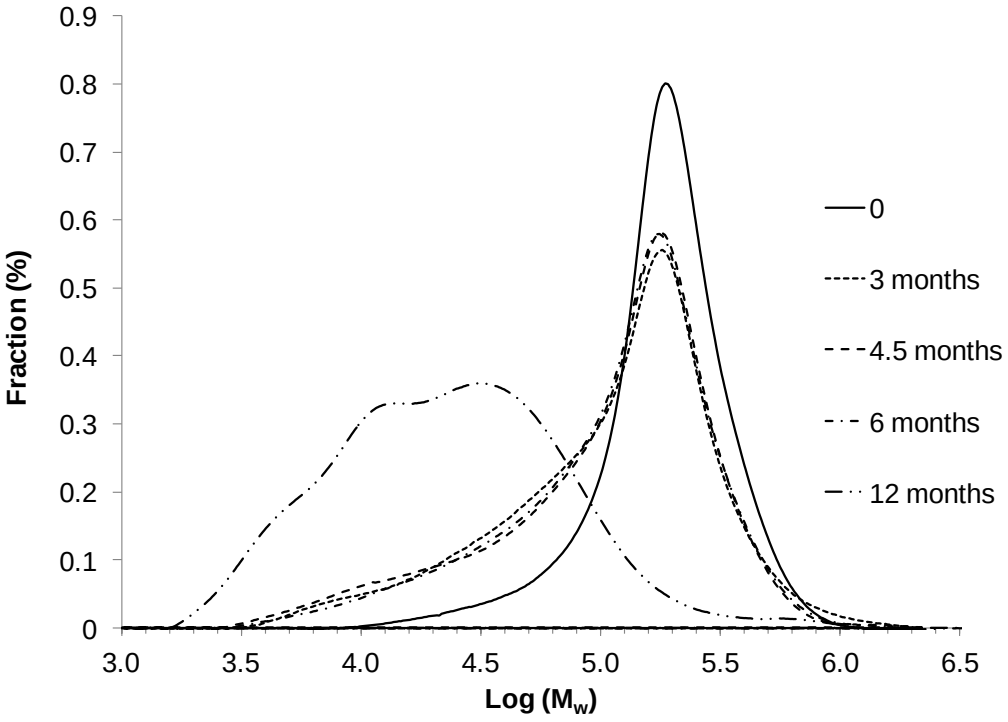

Fig. 4 – GPC curves representing the fraction of chains in percentage as a function of log (M_w) of the PLLA scaffolds after 0, 3, 4.5, 6 and 12 months of hydrolytic degradation.

Table 3–Weight average molar mass (Mw) and polydispersity index (Mw/Mn) after different hydrolytic degradation times in PBS at 37 ºC.

Degradation Time (months)	**Mw (kDa)**	**Mw/Mn**
$t_0 = 0$	165.4	1.4
$t_1 = 3$	126.4	2.3
$t_2 = 4.5$	125.2	2.4
$t_3 = 6$	127.6	2.2
$t_4 = 12$	34.4	2.7

Thermogravimetric analysis

The PLLA scaffolds were thermally degraded in order to evaluate the effect of hydrolytic degradation in PBS on the thermal stability of the polymer chains. The TGA curves shown in Fig. 5a represent the residual mass of the thermally degraded scaffolds. The first derivative of mass as a function of temperature (dw/dT) is also shown in Fig 5b. The derivative curve for non-degraded PLLA indicates that PLLA decomposition takes place in only one step, as it presents only one peak. The maximum peak temperature is seen to gradually lower with degradation time; being 360ºC for non-degraded scaffold and 315 ºC after 1 year's degradation. The non-degraded scaffold starts to thermally degrade around 300 ºC, while the 1-year hydrolytically degraded product starts this process around 210 ºC (Fig. 5a).

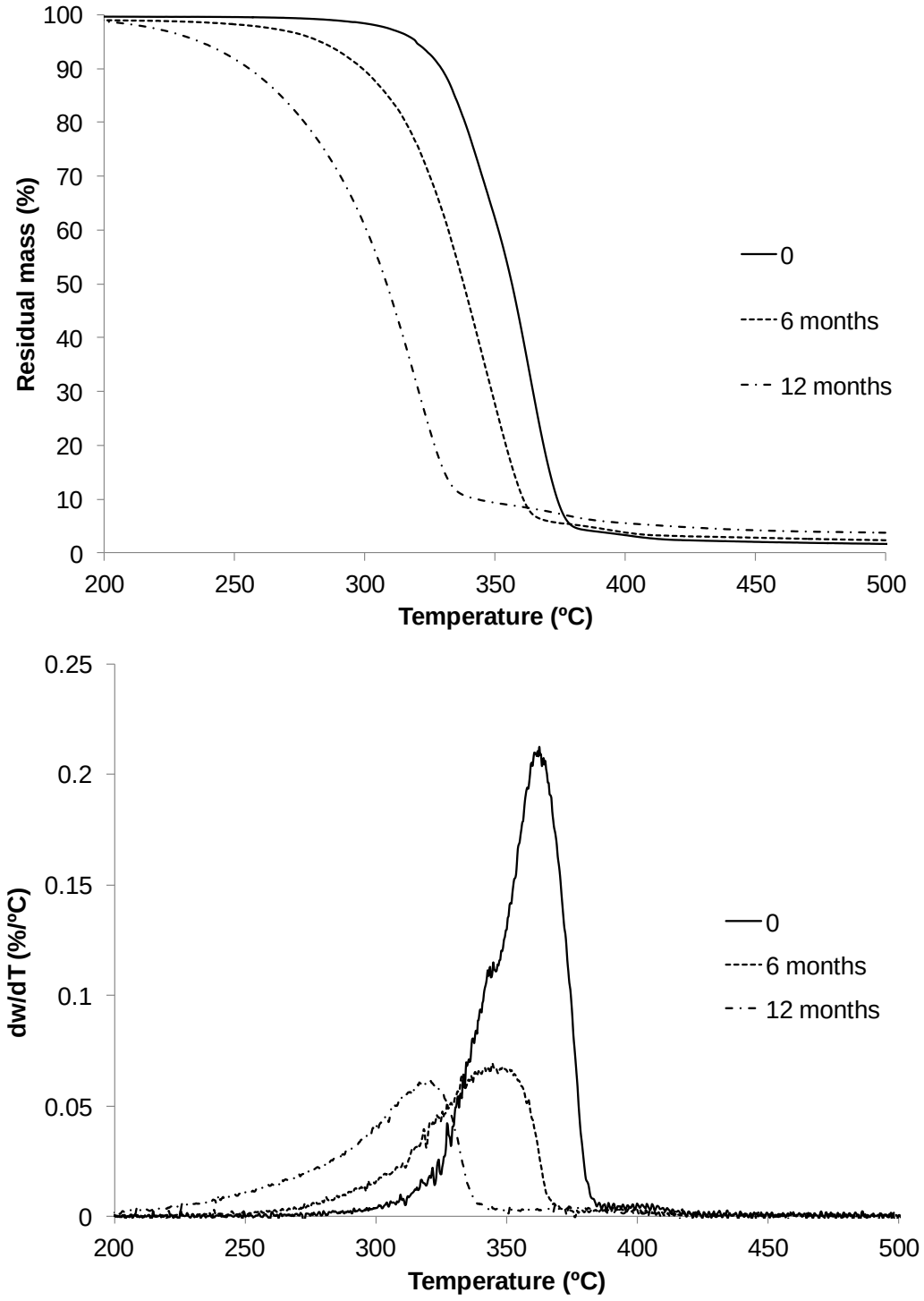

Fig. 5 – (A) Residual mass as a function of temperature of PLLA scaffolds after 0, 6 and 12 months of hydrolytic degradation, and (B) first derivative curves of residual mass with temperature (dw/dT) as a function of temperature for the same samples and conditions.

DISCUSSION

The degradation of the polymer chains can be detected by GPC analysis from the first 3 months (Fig. 4). Although the SEM microphotographs do not clearly show that degradation starts on the pore surface (Fig. 1), microCT images show that macropore dimensions increase with time (Table 1), which is consistent with the rise in permeability. The GPC curves show that a major fraction of chains keeps its molecular weight, as the principal peak of the degraded samples does not change its position but does fall in intensity (Fig. 5). This evolution, together with the increased macropore dimensions and permeability, is characteristic of polymers with surface degradation and is related to PLLA hydrophobicity. PLLA hydrolysis produces carboxylic end groups that favor water penetration into the bulk material. After one year, the GPC curve shifts towards a lower molecular weight as the entire volume of the material becomes affected by the degradation process. The evolution of the molecular weight with degradation time is consistent with previous results obtained by Tsuji *et al*. for crystallized PLLA.[28] The weight loss, however, is the least notable effect in the degradation test, suggesting that the degraded chains remain entrapped in the material, protected by the crystalline regions. The low degradation rate, together with the increasing permeability makes this scaffold suitable for bone regeneration. In our previous work on animal implantation[36] the scaffold maintained the mechanical integrity and stability and allowed the new tissue formation after 6 weeks of implantation in the subchondral bone of sheep.

.

Degradation affects the scaffold's mechanical properties. As shown in Table 1, the Young's modulus (E_s), like the Poisson rate, decreases with degradation time (27 % and 15 % after 6 months, respectively), after which the porous structure loses its biaxial deformation capacity. Moreover, samples reach the plasticization limit at lower deformation levels, since the lower yield limit decreases with degradation time.

The aggregate modulus (H_A), also decreases with degradation time (44% after 6 months). The difference between E_S and H_A was reduced with degradation time, and consequently the Poison coefficient decreases with degradation time. The transition to the plastic region, measured through Y_L in the confined test, remained approximately constant for the 3 first months of degradation. However between 4.5 and 6 months this zone moved toward higher deformation levels. In many applications, as for example in articular cartilage replacement, the scaffold works in a confined space, so that the confined results are more important than those of the unconfined test.

The freeze extraction process generates highly crystallized scaffolds (50 %) (Table 1) without the ability to crystallize further during the first heating scan, so no cold crystallization peak is observed. No significant change in crystallinity with degradation time was observed in the first heating scan. This could be because the degraded chains, which usually belong to the amorphous regions, remain immobile, trapped between the crystalline regions. However, crystallinity was seen to increase in the second heating scan. After melting, the shorter chains produced by degradation, have higher mobility and can reorganize into crystallites. The second heating scan showed the degradation effect through increased crystallinity. Degradation had no significant effect on scaffold T_g,

which is consistent with the results obtained by Tsuji *et al*. on hydrolytic degradation of PLLA in PBS.[31] Previous degradation studies on PLLA porous samples with lower initial crystallinity[15] found higher degradation rate (30% weight loss after 40 weeks) and an increase in crystallinity with degradation time.

The scission of the polymer chains measured by GPC also influences the thermal stability of the samples (Fig. 5a). Persenaire *et al*.[58] describe the influence of molecular weight on PCL thermal degradation. In the case of PLLA, the shift observed in the temperature of the derivative peak could be a consequence of two phenomena. Firstly, the presence of a higher proportion of carboxylic and hydroxilic groups in the degraded samples could act as catalyzers in the scission of ester bonds. Secondly, as the degraded samples have shorter chains, the diffusion of volatile species should be easier and the onset of mass loss is produced at lower temperatures.

The evolution of the properties presented at this work suggests that the polymer is on its first stage of degradation, at least during the 12 months of the experiment. There are signs of transition towards the second degradation stage around 12 months as indicated by the morphological and mass changes.

CONCLUSIONS

The freeze extraction fabrication process led to highly crystalline scaffolds that were able to maintain their morphology after 6 months of static degradation. Macroporosity seemed to be affected by degradation, but no change in microporosity could be observed. Although the morphological changes in the

form of surface erosion were quite slight, when testing the samples in the permeameter the more degraded samples suffered higher surface erosion and consequently permeability considerably increased with degradation time. The scaffolds' high molecular weight and crystallinity made them highly resistant to degradation and no changes in the mass or crystallinity measured in the first scan were observed after one year of degradation. Although degradation attacked the amorphous phase, the degraded chains were trapped in the samples between the crystalline regions. Degradation produced shorter chains with higher mobility, producing the increased crystallinity observed in the second heating scan and a decrease in scaffold thermal stability during degradation. Hydrolytic degradation of PLLA was seen to affect its mechanical properties, as the main parameters (E_S, H_A, v, and Y_L) decreased with degradation time.

ACKNOWLEDGMENTS

The authors acknowledge the support of the Instituto de Salud Carlos III, MINECO and European Commission through the FP7-ERANet EuroNanoMed 2011 PI11/03032 and the FP7-PEOPLE-2012-IAPP with grant agreement PIAP-GA-2012-324386 projects. CIBER-BBN is an initiative funded by the VI National R&D&i Plan 2008–2011, Iniciativa Ingenio 2010, and Consolider Program. CIBER actions are financed by the Instituto de Salud Carlos III with assistance from the European Regional Development Fund. The authors also thank the Tissue Characterization Platform of the CIBER-BBN for its technical support. We would like to thank the Linguistic Assistance Services of the Language Centre- Universitat Politecnica de Valencia for their help in revising this paper.

REFERENCES

1. Zhao, J.; Yuan, X.; Cui, Y.; Ge, Q.; Yao, K. J Appl. Polym. Sci. **2004**, 91,1676-1684.
2. Hutmacher, D. J. Biomater. Sci-Polym Edition. **2001**, 12, 107-124.
3. Butler, D.; Goldstein, S.; Guilak, F. J Biomech Eng-Trans Asme. **2000**, 122, 570-575.
4. Budyanto, L.; Goh, Y. Q.; Ooi, C. P. J. Mater. Sci-Mater. Med. **2009**, 20, 105-111.
5. Woodruff, M. A.; Lange, C.; Reichert, J.; Berner, A.; Chen, F.; Fratzl, P.; Schantz, J.; Hutmacher, D. W. Mater. Today. **2012**, 15, 430-435.
6. Hollister, S. Nat. Mater. **2005**, 4, 518-524.
7. Hutmacher, D. Biomaterials. **2000**, 21, 2529-2543.
8. Chiquet, M.; Reneda, A.; Huber, F.; Fluck, M. Matrix Biology **2003**, 22, 73-80.
9. Diego, R. B.; Estelles, J. M.; Sanz, J. A.; Garcia-Aznar, J. M.; Sanchez, M. S. J. Biomed. Mater. Res. Part B-Appl. Biomater. **2007**, 81B, 448-455.
10. Pitt, C.; Chasalow, F.; Hibionada, Y.; Klimas, D.; Schindler, A. J. Appl. Polym. Sci. **1981**, 26, 3779-3787.
11. Lu, L.; Peter, S.; Lyman, M.; Lai, H.; Leite, S.; Tamada, J.; Vacanti, J.; Langer, R.; Mikos, A. Biomaterials **2000**, 21, 1595-1605.
12. Lu, L.; Peter, S.; Lyman, M.; Lai, H.; Leite, S.; Tamada, J.; Uyama, S.; Vacanti, J.; Langer, R.; Mikos, A. Biomaterials **2000**, 21, 1837-1845.
13. Li, S,; Garreau, H;, Vert, M. J. Mater. Sci: Mater. Med. **1990**,1, 123-130.
14. Odelius, K.; Hoglund, A.; Kumar, S.; Hakkarainen, M.; Ghosh, A. K.; Bhatnagar, N.; Albertsson, A. Biomacromolecules **2011**, 12, 1250-1258.
15. Gong, Y.; Zhou, Q.; Gao, C.; Shen, J. Acta Biomater. **2007**, 3, 531-540.
16. Zhao, J.; Han, W.; Tu, M.; Huan, S.; Zeng, R.; Wu, H.; Cha, Z.; Zhou, C. Mat. Sci. Eng. C **2012**, 32, 1496-1502.

17. Hakkarainen, M.; Albertsson, A.; Karlsson, S. Polym. Degrad. Stab. **1996**, 52, 283-291
18. Zhang, X.; Espiritu, M.; Bilyk, A.; Kurniawan, L. Polym. Degrad. Stab. **2008**, 93, 1964-1970.
19. Chen, J.; Chu, B.; Hsiao, B. S.. Biomaterials **2003**, 24, 1167-1173.
20. Thomson, R.; Wake, M.; Yaszemski, M.; Mikos, A. Biopolymers II **1995**, 122, 245-274.
21. Lee, H.; Jin, G.; Shin, U. S.; Kim, J.; Kim, H. J. Mater. Sci: Mater. Med. **2012**, 23, 1271-1279.
22. Li, W, ;Tuan, R. Macromol. Symp **2005**, 227, 65-75.
23. Ma, J.; He, X.; Jabbari, E. Ann. Biomed. Eng. **2011**, 39, 14-25.
24. Dai, L,; Li, D,; He, J. J. Appl. Polym. Sci. **2013**, 130, 2257-2264.
25. Vieira, A. C.; Vieira, J. C.; Ferra, J. M.; Magalhaes, F. D.; Guedes, R. M.; Marques, A. T. J. Mech. Behav. Biomed. Mat. **2011**, 4, 451-460.
26. Kang, Y.; Yin, G.; Luo, L.; Wang, K.; Zhang, Y. ASBM7: Adv. Biomater. VII **2007**, 342-343, 273-276.
27. Gaona, LA,; Gómez Ribelles, JL,; Perilla ,JE,; Lebourg, M. Polym. Degrad. Stab. **2012**, 97, 1621-1632.
28. Tsuji, H.; Mizuno, A.; Ikada, Y. J. Appl. Polym. Sci. **2000**, 77, 1452-1464.
29. Tsuji, H.; Ikada, Y. Polym. Degrad. Stab. **2000**, 67, 179-189.
30. Freyman, T.M.; Yannas, I.V.; Gibson L.J. Progr. Mater. Sci. **2001**, 46, 273-282.
31. Li, SH.; de Wijn, JR.; Li, JP.; Layrolle, P.; de Groot, K. Tissue. Eng. **2003**, 9, 535-548.
32. Wagoner Johnson A.J.; Herschler B.A. Acta Biomater. **2011**, 7, 16-30
33. Rezwan, K.; Chen, Q.; Blaker, J.; Boccaccini A. Biomaterials **2006**, 27, 3413-3431

34. Acosta Santamaría, V.; Deplaine, H.; Mariggió, D.; Villanueva-Molines, A.R.; García-Aznar, J.M.; Gómez Ribelles, J.L.; Doblaré, M.; Gallego Ferrer, G.; Ochoa, I. J. Non-Cryst. Solids **2012**, 358, 3141–3149.
35. Izal, I.; Aranda, P.; Ripalda, P.; Sanz-Ramos, P.; Mora, G.; Granero-Moltó, F.; Deplaine, H.; Gómez-Ribelles, J.L.; Gallego Ferrer, G.; Acosta, V.; Ochoa, I.; García-Aznar, J.M.; Andreu, E.J.; Monleón-Pradas, M.; Doblaré, M.; Prósper, F. Knee Surg. Sport. Tr. A. **2013**, 21, 1737-1750.
36. Deplaine, H.; Lebourg, M.; Ripalda, P.; Vidaurre, A.; Sanz-Ramos, P.; Mora, G.; Prósper, F.; Ochoa, I.; Doblaré, M.; Gómez Ribelles, J.L.; Izal-Azcárate, I.; Gallego Ferrer, G. J. Biomed. Mater. Res. B **2013**, 101B, 173-186.
37. Lebourg, M.; Suay Anton, J.; Gomez Ribelles, J. L. J. Mater. Sci: Mater. Med. **2010**, 21, 33-44.
38. Ho, M.; Kuo, P.; Hsieh, H.; Hsien, T.; Hou, L.; Lai, J.; Wang, D. Biomaterials **2004**, 25, 129-138.
39. Alberich-Bayarri, A.; Moratal, D.; Escobar Ivirico, J. L.; Rodriguez Hernandez, J. C.; Valles-Lluch, A.; Marti-Bonmati, L.; Mas Estelles, J.; Mano, J. F.; Monleon Pradas, M.; Gomez Ribelles, J. L.; Salmeron-Sanchez, M. J. Biomed. Mater. Res. B **2009**, 91B, 191-202.
40. Mollica, F.; Ventre, M.; Sarracino, F.; Ambrosio, L.; Nicolais, L. Comput. Math. Appl. **2007**; 53, 209-218.
41. Charles, HT. Ann. NY Acad. Sci. **2006**; 1068, 429-446.
42. Harley, BA.; Leung, JH., Silva, E.C.C.M.; Gibson, LJ. Acta Biomater. **2007**, 3(4), 463-474.
43. Mark, R.; DiSilvestro, J. J. Biomech. **2001**, 34, 519–525.
44. Jurvelin, J.S.; Buschmannf, M.D.; Hunziker, E.B. J. Biomech. **1997**, 30(3), 235-241.
45. Korhonen, R.; Laasanen, M.; Toyras, J.; Rieppo, J.; Hirvonen, J.; Helminen, H.; Jurvelin, J. J. Biomech. **2002**, 35, 903-909.

46. Acosta Santamaría, V.A.; García Aznar, J.M.; Ochoa, I.; Doblare, M. Exp. Mech. **2013**, 53, 911-917.
47. Ochoa, I.; Sanz-Herrera, J.A.; Garcia-Aznar, J.M.; Doblare, M.; Yunos, D.M.; Boccaccini, A.R. J. Biomech. **2009**, 42, 257-260.
48. Chor, M.V.; Li, W. Meas. Sci. Technol. **2007**, 18(1), 208–216.
49. Al-Munajjed, A. A.; Hien, M.; Kujat, R.; Gleeson, J. P.; Hammer, J. J. Mater. Sci: Mater. Med. **2008**, 19, 2859-2864.
50. O'Brien, F.J.; Harley, B.A.; Waller, M.A.; Yannas, I.; Gibson, L.J.; Prendergast, P. Technol Health Care **2007**, 15(1), 3-17.
51. Sanz, J.A.; Kasper, C.; van Griensven, M.; Garcia-Aznar, J.M.; Ochoa, I.; Doblare, M. J. Biomed. Mater. Res. B **2008**, 87B(1), 42-48.
52. Truscello, S.; Kerckhofs, G.; Van Bael, S.; Pyka, G.; Schrooten, J.; van Oosterwyck, H. Acta Biomater. **2012**, 8(4), 1648-1658,
53. Castilla-Cortazar, I.; Mas-Estelles, J.; Meseguer-Duenas, J. M.; Escobar Ivirico, J. L.; Mari, B.; Vidaurre, A. Polym. Degrad. Stab. **2012**, 97, 1241-1248
54. Tsuji, H.; Ikada, Y. Polymer **1996**, 37, 595-602
55. Lebourg, M.; Suay Anton, J.; Gomez Ribelles, J. L. Eur. Polym. J. **2008**, 44, 2207-2218
56. Hernández Sánchez, F.; Molina Mateo, J.; Romero Colomer, F.; Salmerón Sánchez, M.; Gómez Ribelles, J.L.; Mano, J.F. Biomacromolecules **2005**, 6, 3291-3299.
57. Hoglund, A.; Odelius, K.; Hakkarainen, M.; Albertsson, A. Biomacromolecules **2007**, 8, 2025-2032.
58. Persenaire, O.; Alexandre, M.; Degee, P.; Dubois, P. Biomacromolecules **2001**, 2, 288-294.

FIGURE CAPTIONS

Fig. 1 SEM pictures at different magnifications and degradation times of the section of the PLLA scaffold showing the effect of static degradation in PBS on scaffold morphology.

Fig. 2 Stress–strain curves of the confined and unconfined uniaxial compression tests after 0, 3, 4.5 and 6 months of static degradation for the PLLA scaffolds.

Fig. 3 Normalized heat flow of the DSC first (1) and second (2) heating scans after 0, 3, 6 and 12 months of static degradation of PLLA scaffolds. The heat flow was normalized by the mass of the samples and the heating rate (10 ºC/min). The arrow represents a unit of heat flow in J/gK.

Fig. 4 GPC curves representing the fraction of chains in percentage as a function of log (M_w) of the PLLA scaffolds after 0, 3, 4.5, 6 and 12 months of hydrolytic degradation.

Fig. 5 (A) Residual mass as a function of temperature of PLLA scaffolds after 0, 6 and 12 months of hydrolytic degradation, and (B) first derivative curves of residual mass with temperature (dw/dT) as a function of temperature for the same samples and conditions.